

Full paper



Heterocyclic polymer supported cathode/Li interface layers to lower the operational temperature of PEO-based Li-batteries

Jingang Zheng^{a,1}, Shaojun Liu^{a,1}, Hao Huang^a, Hongxu Zhou^a, Hongyang Li^a, Lixiang Li^{a,*}, Guangshen Jiang^a, Han Zhang^a, Xin Geng^a, Baigang An^a, Chengguo Sun^{a,b,**}

^a School of Chemical Engineering, University of Science and Technology Liaoning, Anshan 114051, PR China

^b School of Chemical Engineering, Nanjing University of Science and Technology, Nanjing, Jiangsu 210094, PR China

ARTICLE INFO

Keywords:

Electrode-electrolyte interface
Heterocyclic polymer
Mixed ionic/electronic conductor
PEO-based Li-batteries

ABSTRACT

High-performance poly (ethylene oxide) (PEO)-based solid-state polymer Li-batteries (SSLBs) at low temperature (≤ 25 °C) is hindered by high interfacial resistance and low ionic conductivity. Herein, we simultaneously construct cathode and anode interface layers via in-situ heat-induced heterocyclic polymerization reaction, where the cathode-electrolyte interface layer (PPL) consists of bromine-doped poly (3,4-ethylene-dioxy-thiophene) (PEDOT), PEO and bis-trifluoromethanesulfonimide (LiTFSI), featuring with mixed ionic/electronic conduction, and the anode-electrolyte interface layer (PVCL) was formed by poly (vinyl carbonate) (PVC), PEO and LiTFSI, having a robust fast ionic conduction. Benefiting from the PEDOT conductivity, high mechanical strength of PVC and good interface affinity aroused by heat-induced reaction, the solid-state PEO-based LiFePO₄||Li cell shows low interfacial resistance of 11.02 Ω that decreased by 92% compared to the cell without interface modification, and delivering a discharge capacity of 164.4 mAh g⁻¹ at 0.1 C (25 °C), as high as 115.9 mAh g⁻¹ at 10 °C. X-ray photoelectron spectroscopy revealed the enrichment of LiF, Li₃N and LiBr on the lithium metal surface after cycling, further enhancing stable cycling Li-batteries. The dual interface-constructed strategy provides a reliable way to resolve the bottle-neck interfacial issues of SSLBs.

1. Introduction

Solid-state polymer Li-batteries (SSLBs) have considerable advantages over organic liquid Li-batteries including inhibiting Li dendrites, and addressing safety and energy density issues [1]. However, using the solid electrolytes instead of the organic liquid electrolyte system results in the high interfacial resistance, because of the inadequate interface contact between electrode materials and electrolyte and the hardly formation of stable SEI film during cell cycling [2]. Generally, the solid-state battery interfaces consist of cathode-electrolyte interface and anode-electrolyte interface. For the cathode-electrolyte interface, the transport of ionic/electronic across the interface is seriously hindered by the loose solid-solid contact, the low interface conductivity, and the lithium depletion in space charge layer, leading to high interface resistance and badly stable cycling of SSLBs [3]. The anode-electrolyte interface depends on the physicochemical property of lithium metal

and electrochemical behavior of Li⁺. The high chemical reactivity and the uneven plating/stripping of lithium usually caused poorly interfacial compatibility, and rapidly growth of Li dendrites [4]. Therefore, solving the interface problems is an urgent demand for further development of low temperature (≤ 25 °C) high-performance SSLBs [5].

In general, the following factors should be considered when designing the artificial interface layers for SSLBs. (i) Providing enough interfacial affinity between electrode and electrolyte to reduce interfacial impedance; (ii) Maintaining rapid reversible ionic/electronic conduction for high-rate charging and discharging; (iii) Having good chemical compatibility and stability with electrode materials to extend the battery cycle life. Until now, various efficient strategies [6] have been applied to interface engineering for cathode electrolyte interface. For instance, in-situ construction method, interface wetting [7], cathode coating [8] and integrated cathode and electrolyte [9] were used to improve interface contact; Tuning interfacial ionic/electronic mixed

* Corresponding author.

** Corresponding author at: School of Chemical Engineering, University of Science and Technology Liaoning, Anshan 114051, PR China.

E-mail addresses: lxli2005@126.com (L. Li), sunyangguo2004@163.com (C. Sun).

¹ These authors contributed equally to this work and should be regarded as co-first authors.

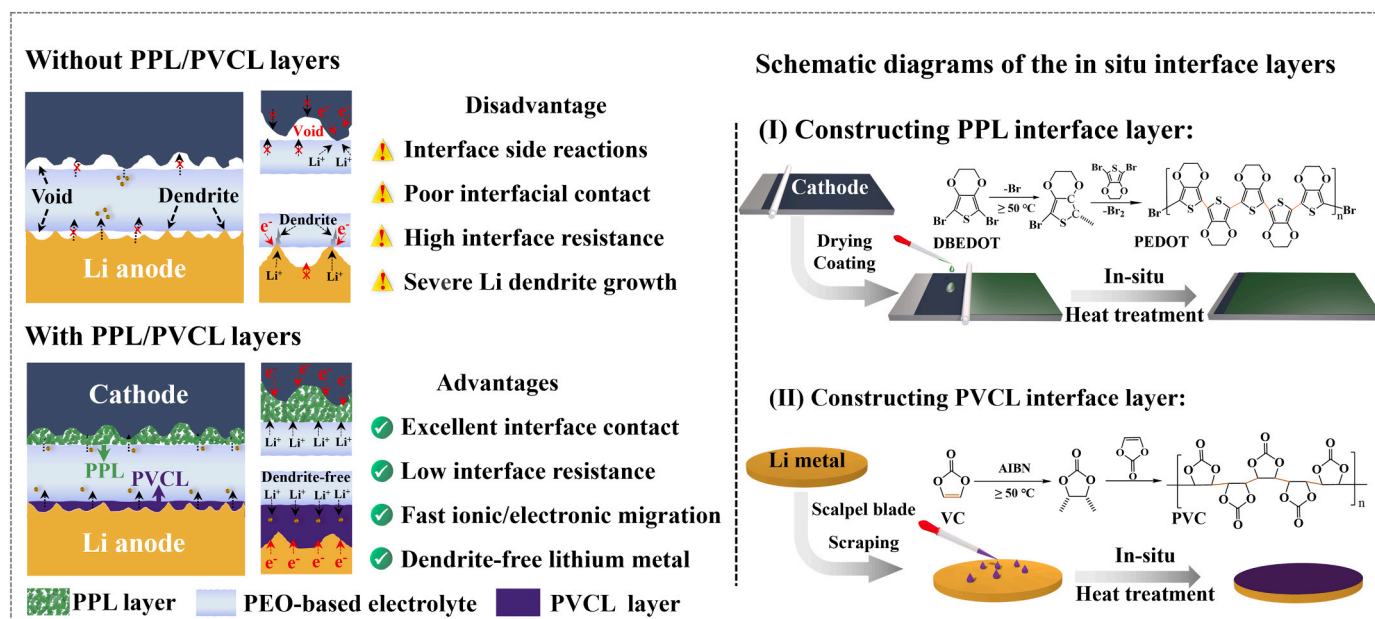


Fig. 1. Illustration of advantages of constructing cathode/anode interface layers, and the construction strategy for both interface layers.

conductor layers has been proved to weaken the influence of space charge layer caused by interfacial ion migration, further enhancing the conduction of interfacial ions [10,11]; Designing asymmetric multilayer electrolytes [12], “polymers-in-salt” electrolytes [13] or introducing the group with high oxidation stability into the electrolyte [14] have the ability to enhance interfacial stability and prolong cycle lifespan of SSLBs. As for anode-electrolyte interface, many advanced techniques, including in-situ alloying of the anode [15], surface modification of solid electrolyte [16] and integration by hot pressing [17], etc. were employed to improve the wettability and compatibility between lithium metal and electrolyte; Atomic or molecular layer deposition [18,19], vacuum evaporation [20] and three-dimensional lithium metal [21] strategies were used to promote interfacial Li^+ migration rate and homogenize plating/stripping to suppress dendrite growth.

Although the above-mentioned interfacial modification techniques have achieved remarkable effects on addressing cathode or anode interface problems, these processes are not friendly to the large-scale manufacturing of SSLBs because of the high cost and the limitation of complicated operations. More importantly, an optimal interfacial strategy should simultaneously consider the cathode and anode interfaces, because the good performance of a battery depends on electrochemical characteristics of each interface layer. However, it is an enormous challenge to concurrently construct the matching interface layers at both cathode and anode interfaces by one-step treatment. To address the problem, we envision the addition of organic monomer additives on both sides of the electrolyte membrane that can easily polymerize with the help of initiators, to create interface buffer layers at cathode and anode sides. Given some of methods often involved in organic polymerization, such as UV-curable polymerization [22], electro-polymerization [23] and ultrasonic resonance polymerization [24]. Heat-induced polymerization has aroused our heightened concern due to the well-controlled reaction conditions and easy operation in the cell manufacturing process. However, there are very few reports exploring the concept in solid-state polymer electrolyte systems, because it appeared to be difficult to obtain suitable heat-induced monomers for both cathode and anode interfaces. After extensive experimentation, we found that the heterocyclic compounds of 2,5-dibromo-3,4-ethylene-dioxythiophene (DBEDOT) and vinylene carbonate (VC) easily occur self-polymerization and exhibit excellent properties in terms of electronic and ionic transport. Specifically, DBEDOT is prone to converted

into conductive PEDOT by facile heat treatment under solid-state condition, and it has been employed to enhance the electrical conductivity of electrodes [25]. Due to the five-membered heterocyclic with conjugated backbones in the molecular structure, PEDOT can resist the risk of decomposition under high voltage (~ 4.6 V vs. Li^+/Li) [26]. Under the same heat treatment condition, VC can undergo self-polymerization to form PVC with the assistance of free radicals, it is electronic insulator but well ionic conductor. For example, the ionic conductivity of PVC mixed with high concentration of LiTFSI can reach 10^{-4} S cm^{-1} at room temperature [8]. Besides, PVC has excellent electrochemical stability and robust mechanical properties, which can provide support for mitigating the volume changes of the anode during cycling and inhibiting dendrite growth.

Herein, we propose the heat-induced polymerization reaction of heterocyclic compounds for in-situ fabricate the cathode and anode interface layers, meeting the required ionic/electronic transport of cathode/anode interfaces. As illustrated in Fig. 1, DBEDOT mixed with PEO and LiTFSI as a monomer component before polymerization was in-situ positioned at the cathode side. After polymerization, the formed PPL layer not only can provide a combined path for Li^+/e^- transport in cathode-electrolyte interface, but also as an interface protection layer suitable for high-voltage cathode materials due to the antioxidative PEDOT. For anode interface, the mixed solution of PVC, PEO and LiTFSI was designed as anode-electrolyte coordinated layer (PVCL) due to its high ionic conductivity of 1.04×10^{-4} S cm^{-1} at room temperature and low Li^+ migration energy barriers (0.18 eV). This in-situ customization of heterocyclic PPL interfacial layer imparts the good interfacial electronic/ionic conductivity for the cathode interface, the PVCL layer achieves the good compatibility with lithium metal interface. In addition, the bromide as the by-product of heterocyclic compound DBEDOT self-polymerization can migrate from the cathode to anode and participate in the formation of SEI layer along with Li_3N and LiF, further enhancing the efficiency and stability of lithium plating/stripping. Our results show that the in-situ customized organic polymer layers can effectively mitigate the interfacial issues between electrodes and solid-state polymer electrolytes.

2. Results and discussion

DBEDOT can be polymerizable in the solid state by heat-induced

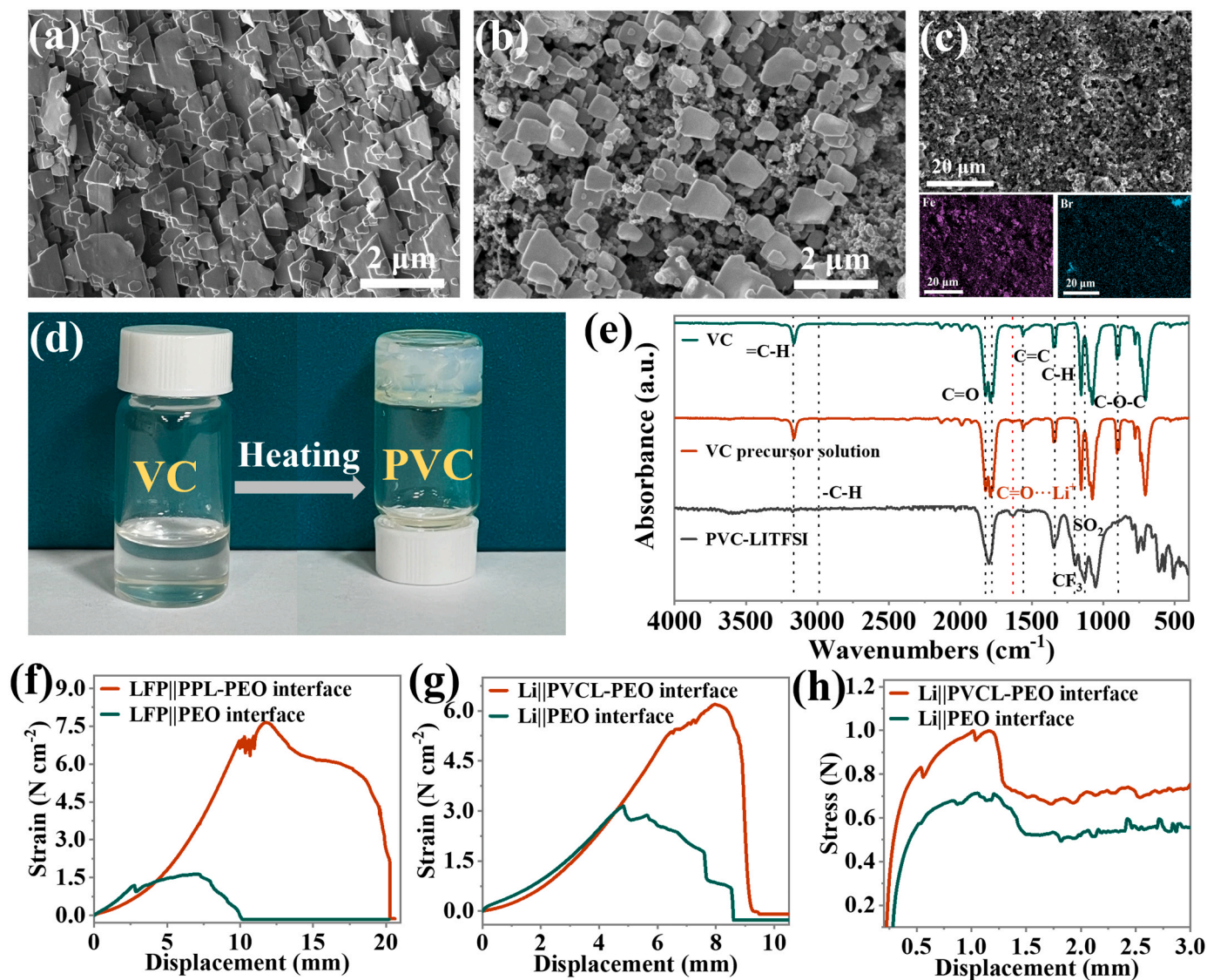


Fig. 2. (a), (b) SEM images of pure PEDOT and in-situ PEDOT on cathode surface. (c) SEM and EDS images of LFP electrode coated by PPL layer. (d), (e) Digital photo and FTIR spectrograms of VC before and after polymerization. (f), (g) Stripping test curves of cathode-electrolyte interface and anode-electrolyte interface. (h) Puncturing test curves of PVCL layer and PEO-based electrolyte.

free-radical reaction. We analysed the differences in morphology between the polymerization of pure DBEDOT under environmental condition and the in-situ polymerization of DBEDOT mixed with PEO and LiTFSI in cells. As shown in Fig. 2a and b, the obtained PEDOT polymer exhibits a sheet-like morphology with a monodispersed structure in both conditions. Due to the control of DBEDOT dosage (~ 0.4 mg) in the cell, the length of PEDOT ranges from 300 nm to 500 nm and the corresponding thickness is around 50 nm (Fig. S1a and b). In contrast to the PEDOT formed at environmental condition, the PEDOT in cell is loosely distributed on the LFP cathode surface without completely covering the surface of LFP electrode to hinder Li^+ transport (Figs. 2b and S1c). The energy dispersive X-ray spectroscopy (EDS) mapping of Fe and Br elements can also verify that the PPL layer can evenly disperse on the surface of LFP cathode (Fig. 2c). Fourier Transform Infrared Spectrometer (FTIR) spectroscopy was performed to observe the evolution of DBEDOT monomer before and after polymerization (Fig. S2). DBEDOT has a typical peak of aromatic C-Br bond at 1082 cm^{-1} , after polymerization, the isolated PEDOT from the electrolyte shows no characteristic peaks due to the lack of the inherent transmittance relevant to the formed PEDOT polymer. The complete disappearance of the C-Br peak suggested that the heat-induced polymerization is performed very well

in solid-state reaction [27]. The detailed comparison of FTIR spectra of PEO-DBEDOT and PEO-DBEDOT membranes before and after polymerization is shown in Fig. S3. As for construction of lithium metal anode interface, AIBN as a heat-induced radical initiator was employed to promote the conversion of liquid VC to polymer at 60°C for 24 h (Fig. 2d). As shown in Fig. 2e, the formation of PVC can be proved by the transformation of $=\text{C-H}$ bond in VC (3164 cm^{-1}) to $-\text{C-H}$ single bond of PVC (2976 cm^{-1}). The enhancement of the peak at 1636 cm^{-1} for the $\text{C}=\text{O}$ bond indicates the strongly coordinated with Li^+ , promoting LiTFSI dissociation into Li^+ and TFSI $^-$ ions, which well matches with previously reported results [8]. To calculate degree of polymerization, the molecular weight and structure of PEDOT and PVC were also determined (Fig. S4-S5). The molecular weight of PVC and PEDOT are 1.56×10^6 and 2168, respectively, and the corresponding XRD patterns reveal that both polymers feature with amorphous structure.

To demonstrate the adhesion and intimacy of interface contact between electrodes and PEO-based electrolyte after in-situ construct interface layers, tensile stripping test of LFP||PPL-PEO interface and PEO-PVCL||Li interface are presented in Fig. 2f and g. For cathode-electrolyte interface, the separating force (fracture energy) is measured about 7.64 N cm^{-2} for LFP||PPL-PEO interface, which is

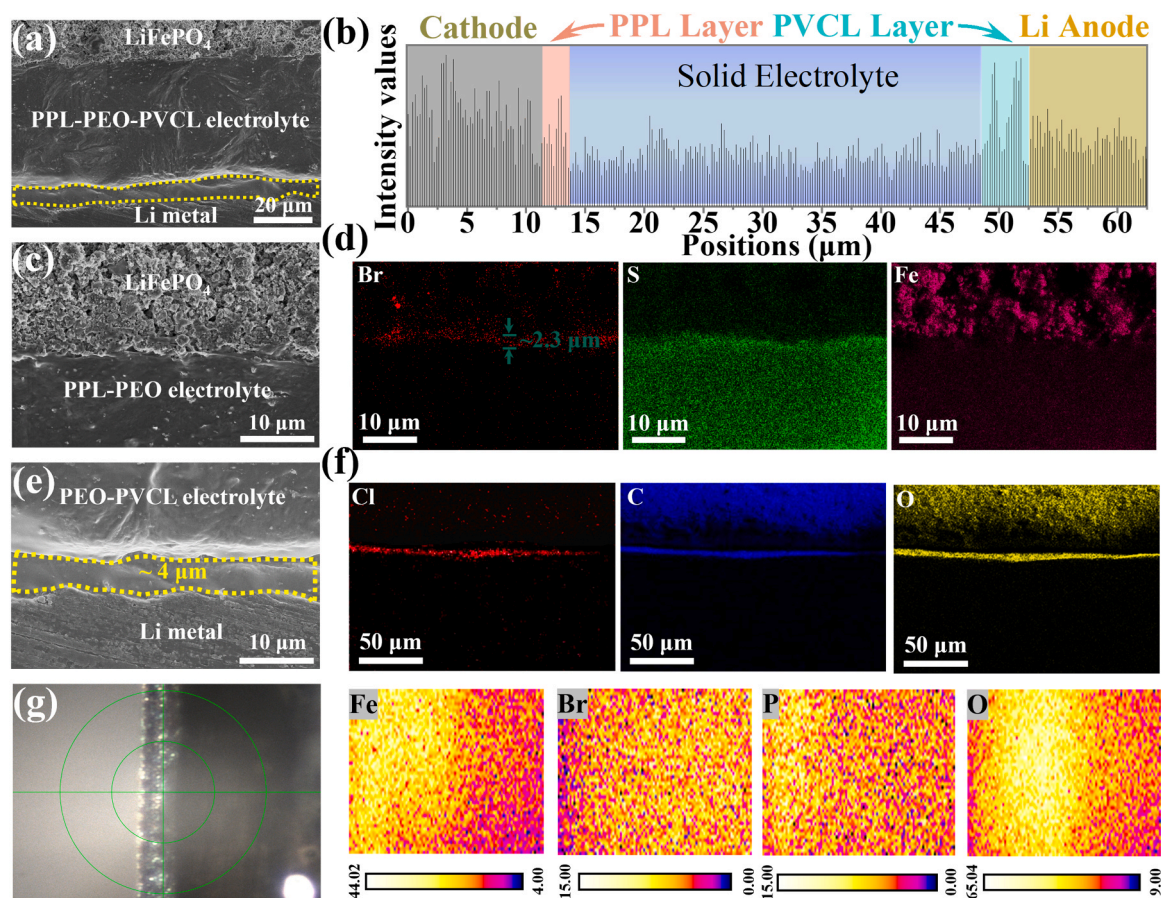


Fig. 3. (a), (b) SEM images of full interfaces and the corresponding signal intensity in different positions. (c) Cross-sectional SEM images of LFP||PPL-PEO interface and (d) Corresponding region of EDS mapping images (Br, S and Fe element). (e), (f) Cross-sectional SEM images and EDS mapping images (Cl, C and O element) of Li||PVCL-PEO interface. (g) Cross-sectional XPS mapping images of LFP||PPL-PEO interface (Fe, O, P and Br element).

higher than LFP||PEO interface (1.63 N cm^{-2}) (Fig. 2 f). As for anode-electrolyte interface, the separating force of the PEO||Li interface and the PEO-PVCL||Li interface are 3.06 and 6.20 N cm^{-2} , respectively (Fig. 2 g). The increase in stripping loading demonstrates that the electrodes and PEO-based electrolyte have intimate contact, which is vital for interface to reduce resistance. To verify the strength of the in-situ interfacial layers, puncturing test for PEO-based electrolyte with and without PVCL layer were performed. As seen in Fig. 2 h, puncturing the PEO-based electrolyte with PVCL layer needed a higher load (1 N) compared to the bare PEO-based electrolytes (0.71 N). The results demonstrate that in-situ construction of PPL and PVCL layers has ability to resist the puncture injury. All these results reflect that construction of double interface layers can achieve good adhesion and robustness between electrodes and electrolyte interfaces, which may have a contribution in reducing interface resistance and improving protection of the electrolyte from damage caused by growth of lithium dendrites.

The characteristics of PPL and PVCL layers within the LFP||PPL-PEO-PVCL||Li cell were also observed. Fig. 3a displays the cross-sectional scanning electron microscope (SEM) images of the cell, it can be found that there is close contact between the electrodes and PEO-based electrolyte, without obvious boundary. As shown in Fig. 3b, based on the variation of the signal intensity with different surface compositions during a full scanning of the whole cross-section, the thicknesses of the in-situ PPL and PVCL layers are approximately $2\text{--}3 \mu\text{m}$ and $4 \mu\text{m}$, respectively. The higher magnification cross-sectional images of the LFP||PPL-PEO interface were presented in Fig. 3c and Fig. S6, further showing the excellent intimate contact. Given the Br element is detected at corresponding interface by EDS mapping, while S and Fe elements are distributed in the corresponding regions of the electrolyte and LFP

electrode, respectively. It indicates that the thickness of the interface layer is about $2.3 \mu\text{m}$ (Fig. 3d), consistent with the results in Fig. 3b. The cross-sectional X-ray photoelectron spectroscopy (XPS) mapping technique was carried out for further observed the gradient variation of elements concentration between LFP electrode and PEO-based electrolyte with in-situ PPL layer. As shown in Fig. 3g, the color of Fe, O, P element images gradually transitions from yellowish white to bluish violet between LFP and PEO-based electrolyte, while the opposite is true for the color transition of Br, due to the former stems from LFP and the Br element is derived from PEDOT. The changes in color from white to blue reflect a decrease in content. The above results imply PEDOT was concentrated in the interface region and tended to seep into the LFP framework. This feature not only facilitates the construction of efficient reversible interface ionic/electronic transfer channels, but also improves the electronic conductivity within the electrode. For PEO-PVCL||Li interface, the cross-sectional SEM image (Fig. 3e) shows that the PVCL layer acts as a “bridge” to contact PEO-based electrolyte and lithium metal anode, and maintains a thickness of interface layer approximately $4 \mu\text{m}$. The result also can be examined by the EDS mapping of PEO-PVCL||Li interface. In Fig. 3f, lithium perchlorate (LiClO_4) was instead of LiTFSI to distinguish the elements of the interface layer. Compared to the distribution of O and C elements, Cl as a characteristic element is only observed at the interface, indicating good compatibility of anode-electrolyte interface is achieved.

Since atomic force microscope (AFM) technique is very powerful to visualize the roughness of given surface, Fig. 4a and b present the visualization of LFP electrode surface with and without PPL layer by AFM. In contrast to the original LFP electrode surface (Fig. 4a), the LFP electrode surface with in-situ PPL layer, depicts a flat plane with less

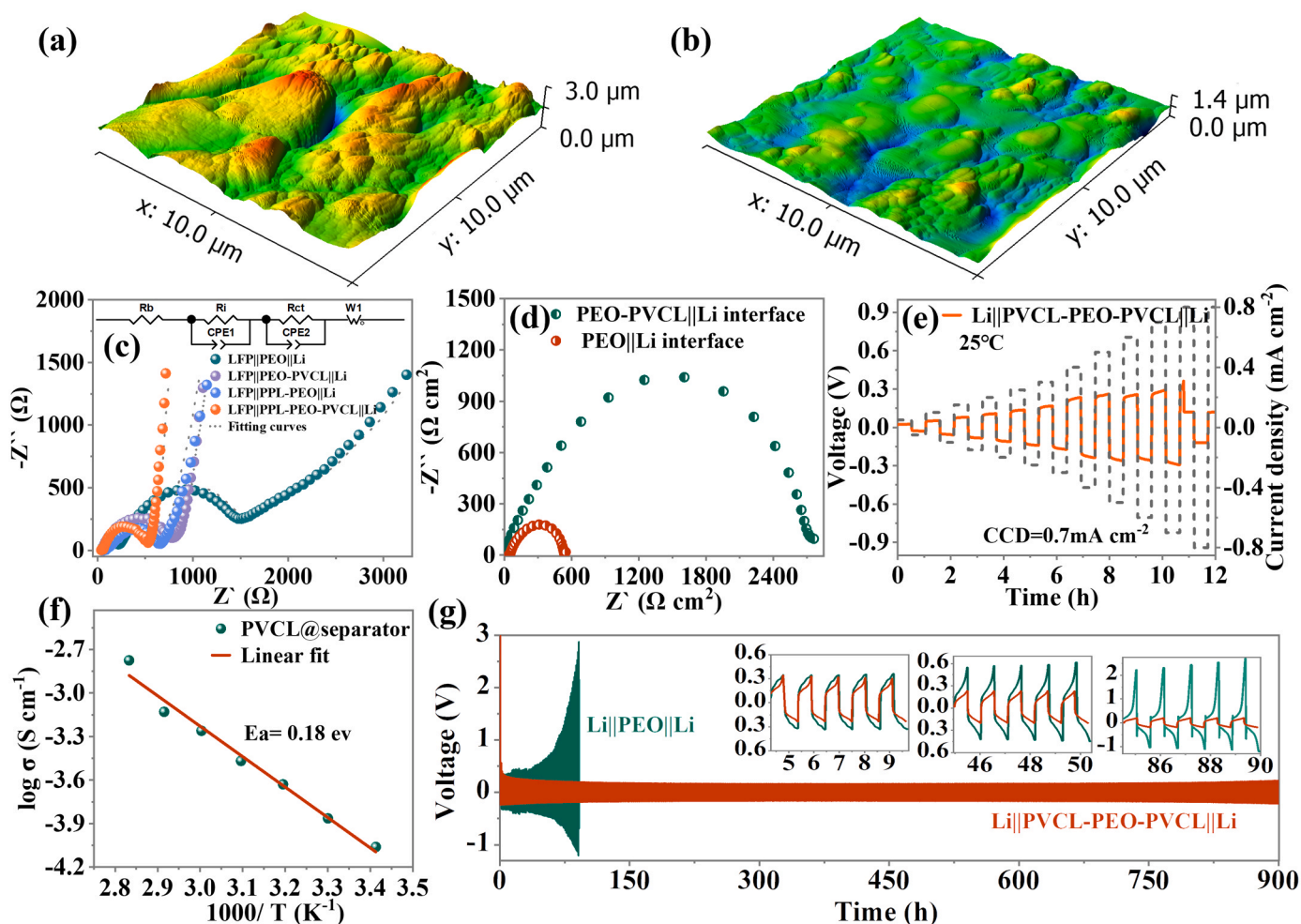


Fig. 4. (a), (b) AFM images of LFP electrode without and with PPL layer. (c) Nyquist impedance plots and equivalent circuits of LFP||Li cells, CPE₁ and CPE₂ are constant phase elements, W₁ is Warburg diffusion. (d) Nyquist impedance plots of Li||PVCL-PEO-PVCL||Li cell and Li||PEO||Li cell at 25 °C. (e) Critical current density of Li||PVCL-PEO-PVCL||Li cell. (f) Temperature-dependent ionic conductivity of PVCL membrane. (g) Lithium plating/stripping test of 0.1 mA cm⁻² at 25 °C.

roughness (Fig. 4b). This will change the Li⁺ conduction mode from point contact to face contact, reducing energy barriers of interfacial ion transport. The ionic and electronic conductivity (σ_i and σ_e) of PPL layer was also measured by electrochemical methods. As shown in Fig. S7, the σ_i and σ_e for PPL are 9.67×10^{-6} S cm⁻¹ and 1.73×10^{-8} S cm⁻¹, respectively, which is much higher than that of PEO electrolyte ($\sigma_i = 3.39 \times 10^{-6}$ S cm⁻¹, $\sigma_e = 4.07 \times 10^{-11}$ S cm⁻¹). The results show that PPL layer has good mixed ionic/electronic transport capability. Electrochemical impedance spectroscopy (EIS) was employed to test the resistance changes of LFP||Li cell with and without PPL/PVCL layers. Fig. 4c shows the resistance curves of four cells with PEO, PPL-PEO, PEO-PVCL and PPL-PEO-PVCL as electrolyte and interface modification layers. Each resistance curve generally consists of four parts: the primarily one is the resistance of the bulk electrolyte (R_b), corresponding to the intersection of the Nyquist plots with x-axis. The interface resistance (R_i) and charge transfer resistance (R_{ct}) are observed as semicircles in the high frequency and mid-frequency regions, respectively; Warburg impedance (W_1) represented by the sloping line was found in the low frequency region. Based on the determined equivalent circuit model (the inset Fig. 4c), the corresponding impedance values for each frequency range were obtained after fitting and listed in Table S1.

It can be found that the R_b of LFP||PEO||Li, LFP||PEO-PVCL||Li, LFP||PPL-PEO||Li and LFP||PPL-PEO-PVCL||Li cells are slight change (47.5–50.2 Ω), the corresponding R_i values varies significantly from 141.7, 45.7 and 23.7 to 11.02 Ω . The significant reduction in R_i further demonstrates the in-situ formed double interface layer is a high-efficient

strategy to regulate interface property. Due to the electronic conduction of PEDOT, the R_{ct} is also decreased from the initial 1051 Ω for LFP||PEO||Li to 495.8 Ω for LFP||PPL-PEO-PVCL||Li. The great change in resistances suggest that in-situ introduction of a mixed ionic/electronic conduction layer at cathode-electrolyte interface can solve the interfacial problems. The formed interlayer can effectively reduce interfacial resistance and provide reversible transport channel for Li⁺/e⁻, allowing a smooth charge transfer process at interface, as well acts as a physical barrier to separate the electrolyte from the high voltage cathode [28].

The Li⁺ exchange reaction at the anode-electrolyte interface was also investigated by EIS method [29]. Fig. 4d shows the resistance curves of Li||PVCL-PEO-PVCL||Li and Li||PEO||Li symmetric cells. The value of Li||PVCL-PEO-PVCL||Li resistance (535.2 Ω cm²) was much smaller than that of Li||PEO||Li (2741 Ω cm²). The EIS in the temperature range of 30 to 70 °C was also fitted according to the Arrhenius law, The calculated the activation energies (E_a) of the PEO-PVCL||Li and PEO||Li interfaces were 0.68 eV and 0.94 eV, respectively (Fig. S8), indicating that with the assistance of the PVCL layer, Li⁺ can more easily access the electrode-electrolyte interface. The high ionic conductivity of PVCL at room temperature (1.04×10^{-4} S cm⁻¹) (Fig. S9) and the corresponding low E_a (0.18 eV) for SS||PVCL||SS (Fig. 4f) further confirm the results. The critical current density (CCD) of the Li||PVCL-PEO-PVCL||Li cell was also evaluated, which can reach 0.7 mA cm⁻² (Fig. 4e), in contrast, the Li||PEO||Li cell is only 0.2 mA cm⁻² (Fig. S10). As seen in Fig. 4g, Li||PVCL-PEO-PVCL||Li cell can maintain stable cycling over 900 h with a smooth overpotential plateau (0.22 V) at 0.1 mA cm⁻². Increasing the

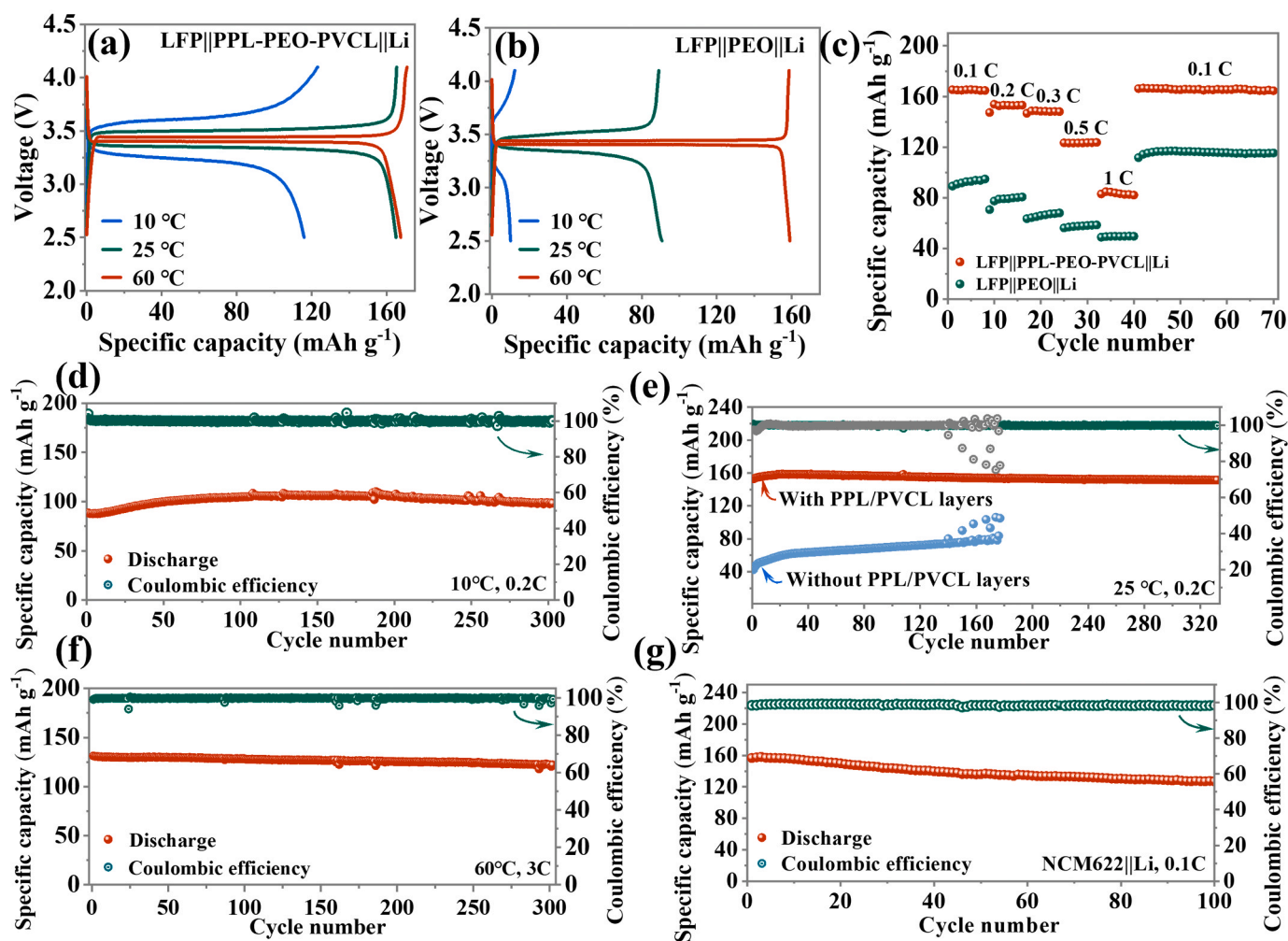


Fig. 5. (a), (b) Charge-discharge curves of LFP||PPL-PEO-PVCL||Li and LFP||PEO||Li cells in the range of 10–60 °C at 0.1 C, respectively. (c) Rate performance of LFP||PPL-PEO-PVCL||Li and LFP||PEO||Li cells at 25 °C. (d) Cycling performances of LFP||PPL-PEO-PVCL||Li cell at 10 °C. (e) Cycling performances of LFP||PEO||Li cell with and without interface layers at 25 °C. (f) Cycling performances of LFP||PPL-PEO-PVCL||Li cell at 60 °C. (g) Cycling performances of NCM622||PPL-PEO-PVCL||Li cell at 25 °C.

current density to 0.2 mA cm⁻¹, it exhibits good stability after 180 h of cycling, without an internal short circuit or a rise in hysteresis potential (Fig. S11). At a high current density of 0.5 mA cm⁻², it still displays stable cycling performance (Fig. S12), demonstrating that the PVCL layer has ability to maintain the stability of the anode-PEO electrolyte interface. However, due to the intrinsic soft mechanical properties and strong interactions of ether oxygen bonds with Li⁺ in the PEO electrolytes, as well as electrochemical reactivity is limited in solid-state polymer electrolyte, the overpotential (~ 1.5 V) and cycling life (109 h) were affected.

The LFP||PEO||Li cells were assembled to examine the effect of PPL/PVCL interface layers on the cell performance. It is worth mentioning that all assembled cells were placed in a 60 °C oven for 24 h to eliminate the influence of high temperature. Fig. 5a presents the voltage curves of the LFP||PPL-PEO-PVCL||Li cell in range of 10 to 60 °C at 0.1 C. It provides a high discharge capacity of 164.7 mAh g⁻¹ at 25 °C and 167.4 mAh g⁻¹ at 60 °C, very approaching the theoretical discharge value of LFP electrode (1 C = 170 mAh g⁻¹). Even at 10 °C, it also can provide a high discharge capacity of 115.9 mAh g⁻¹. In contrast, the LFP||PEO||Li cell without PPL/PVCL layers hardly can work regularly at 10 °C, the discharge capacity is only 10 mAh g⁻¹ (Fig. 5b), even at 25 °C, it still delivers a low discharge capacity of 90.8 mAh g⁻¹, until the temperature rises to 60 °C, due to the softening of the PEO-based electrolyte and the improvement of electrode-electrolyte interface contact, it can deliver a

high discharge capacity of 159 mAh g⁻¹. As shown in Fig. 5c, the LFP||PPL-PEO-PVCL||Li cell displays excellent rate capability at 0.5 (123.4 mAh g⁻¹) and 1 C (84.8 mAh g⁻¹). When the current density switched back to 0.1 C, the capacity was restored to 166.6 mAh g⁻¹. However, the LFP||PEO||Li cell only presented 58.1 and 49.6 mAh g⁻¹ at 0.5 C and 1 C, respectively (Fig. S13). Fig. 5d-f present the long-term cycling in range of 10 to 60 °C. The LFP||PPL-PEO-PVCL||Li cell delivers a high discharge capacity of 98.4 mAh g⁻¹ after 300 cycles at 10 °C (0.2 C) (Fig. 5d), and 155 mAh g⁻¹ after 330 cycles at 25 °C (Fig. 5e). At higher rates of 0.3 C and 0.5 C, it also exhibits a long cycle life with the high discharge capacity of 152 mAh g⁻¹ and 130.6 mAh g⁻¹, respectively (Fig. S14). On the contrary, the LFP||PEO||Li cell shows a rapid drop in coulombic efficiency after 140 cycles at 25 °C (0.2 C), only provide a low discharge capacity of 80 mAh g⁻¹ (Fig. 5e). At 60 °C, the LFP||PPL-PEO-PVCL||Li cell still has a high initial discharge capacity of 131.3 mAh g⁻¹ at high rate of 3 C, and the capacity retention rate is 93.15% after 300 cycles (Fig. 5f). Because of the in-situ fabrication of PPL/PVCL interface layer promotes the tight contact between cathode/anode and electrolyte, the “double strategy” can provide high ionic conductivity to 1.025 × 10⁻⁴ S cm⁻¹ (Table S2), low E_a of 0.16 eV and satisfied lithium transference number (0.47) for PEO-based electrolytes (Figs. S15 and S16). Besides, benefitting from the excellent interface performance, the cell also can be charged and discharged smoothly at high loading of cathode materials between 5 and

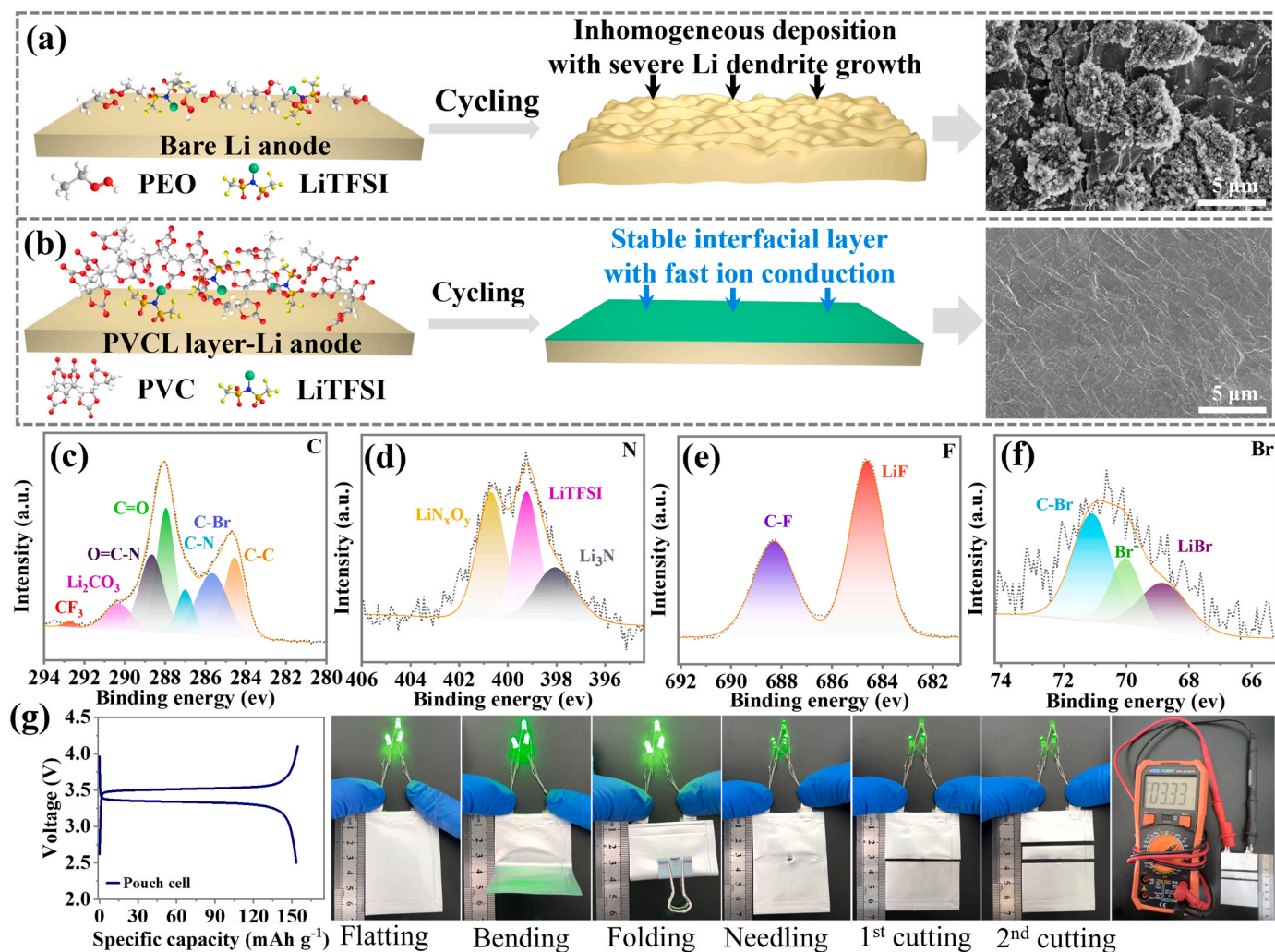


Fig. 6. (a), (b) Schematic illustration of the Li plating and the corresponding SEM images of lithium metal anodes after cycling. (c), (d), (e) (f) XPS analysis of lithium metal anode of LFP||PPL-PEO-PVCL||Li cell after 50 cycles at 0.2 C (C, N, F, Br elements). (g) Charge/discharge curves of LFP||PPL-PEO-PVCL||Li pouch cell at 0.1 C (25 °C) and lighting LED lamps under extreme conditions.

10 mg cm⁻² (Fig. S17). Owing to the PPL/PVCL layers extend the electrochemical window up to 4.6 V (Fig. S18), the high-voltage LiNi_{0.6}Mn_{0.2}Co_{0.2}O₂||PPL-PEO-PVCL||Li cell delivers a high discharge capacity of 151.7 mA h g⁻¹ at 0.1 C and maintains at 127 mA h g⁻¹ after 100 cycles (Fig. 5 g).

To understand the positive effect of PVCL layer on lithium plating/stripping. Surface morphologies of the lithium metal anodes disassembled from Li symmetric cell after 50 cycles at 0.2 mA cm⁻². As shown in Fig. 6a, for Li||PEO||Li cell, massive byproducts with large and uneven grain sizes were produced on the surface of lithium metal anode, originating from the aggregation of nanoparticles by inhomogeneous lithium deposition during cycling. Notably, the lithium metal anode with PVCL layer after cycling exhibits a smooth surface and uniformly dispersed nanoparticles with no visible dendrites (Fig. 6b), indicating the in-situ heterocyclic PVCL layer can effectively stabilize lithium metal.

The lithium metal surface compositions of LFP||PPL-PEO-PVCL||Li cell was measured by XPS. As can be seen in Fig. 6c-f, the inorganic SEI membrane components, including Li₂CO₃ (290.36 eV, C 1 s), Li₃N (398.04 eV, N 1 s), LiF (684.61 eV, F 1 s) decomposed from LiTFSI were observed. It is worth mentioning that the LiBr (68.82 eV, Br 3d) was detected as well. We concluded that Br element is derived from by-product of DBEDOT self-polymerization, and Br⁻ migrates from the cathode to anode during charging and discharging. As far as the anode

additive is concerned, the bromide is beneficial to form the stable SEI and suppress Li dendrite growth [30]. This implies that the PVC, lithium metal, and the decomposition products may act synergistically to form uniform coverage of interfacial layer, providing a tight interfacial contact and homogeneous lithium plating/stripping. The formed interfacial barrier layer makes PEO-based electrolyte effectively resist the erosion of chemical reaction during cycling. To confirm the feasibility of the PPL/PVCL heterocyclic layers, an LFP||PPL-PEO-PVCL||Li pouch cell with N/P ratio of ~17 was assembled. It can exhibit a high initial discharge capacity of 153.3 mA h g⁻¹ at 0.1 C without obvious capacity decay after 100 cycles (Fig. S19). After suffering a series of abuse tests, including bending, folding, needling, and multiple cutting, the pouch cell still maintains a stable output voltage of 3.33 V and make LED lamps lighting (Fig. 6g). All results reveal that the strategy of regulating cathode/anode interfaces synchronously holds great potential in developing high performance SSLBs at low temperature.

3. Conclusions

We have demonstrated a strategy to significantly solve the interfacial issues of PEO-based Li-battery by construction of double heterocyclic layers at cathode/anode interfaces. A flexible PPL layer with mixed ionic/electronic conduction properties were in-situ formed at cathode interface, achieving low interface resistance and highly stable contact

between cathode and PEO-based electrolyte. Simultaneously, a robust PVCL layer with high Li^+ conductivity ($1.04 \times 10^{-4} \text{ S cm}^{-1}$) and low Li^+ migration energy barriers (0.18 eV) was incorporated into anode interface, ensuring the stable interfacial compatibility and uniform lithium plating/stripping between anode and PEO-based electrolyte. Further exploring the effect on PEO-based Li-batteries performance, $\text{LiFePO}_4||\text{PPL-PEO-PVCL}||\text{Li}$ cell displayed high discharge capacity and good cycle stability at 0.2 C of 10 °C, demonstrating that the modify of double interface layers has ability to reduce the interfacial ion transport resistance, enabling the PEO-based electrolyte to exhibit excellent electrochemical performance at low temperature. This customized strategy for individual requirements of cathode/anode will be a promising technology to address the charge dynamics within the batteries, including electrode structure, electrode-electrolyte interfaces, and solid-state electrolytes with fast ion transport capabilities.

Supporting Information

Detailed experimental methods, molecular weight determination, structural analysis, and additional electrochemical performance and charge-discharge curves.

CRediT authorship contribution statement

Jingang Zheng: Writing – original draft, Data curation. **Shaojun Liu:** Data curation, Formal analysis. **Hao Huang:** Methodology, Writing – original draft. **Hongxu Zhou:** Investigation, Validation. **Hongyang Li:** Investigation. **Guangshen Jiang:** Conceptualization, Visualization. **Han Zhang:** Supervision. **Lixiang Li, Xin Geng:** Validation, Visualization. **Baigang An:** Writing – review & editing. **Chengguo Sun:** Supervision, Funding acquisition, Validation.

Declaration of Competing Interest

The authors declare that they have no known competing financial interests or personal relationships that could have appeared to influence the work reported in this paper.

Data availability

Data will be made available on request.

Acknowledgments

The authors gratefully acknowledge financial supported by the National Natural Science Foundation of China (11972178, 51972156, 52371224 and 21701077), the Talent Project of Revitalizing Liaoning (XLYC1807114).

Appendix A. Supporting information

Supplementary data associated with this article can be found in the online version at [doi:10.1016/j.nanoen.2023.108975](https://doi.org/10.1016/j.nanoen.2023.108975).

References

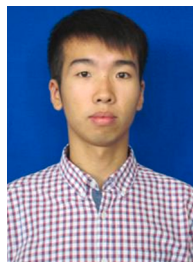
- M. Lee, J. Han, K. Lee, Y. Lee, B. Kim, K.-N. Jung, B.J. Kim, S. Lee, Elastomeric electrolytes for high-energy solid-state lithium batteries, *Nature* 601 (7892) (2022) 217–222, <https://doi.org/10.1038/s41586-021-04209-4>.
- H.-D. Lim, J.-H. Park, H.-J. Shin, J. Jeong, J. Kim, K.-W. Nam, H.-G. Jung, K. Chung, A review of challenges and issues concerning interfaces for all-solid-state batteries, *Energy Storage Mater.* 25 (2020) 224–250, <https://doi.org/10.1016/j.ensm.2019.10.011>.
- C. Chen, M. Jiang, T. Zhou, L. Rajmakers, E. Vezhlev, B. Wu, T. Schüllli, D. Danilov, Y. Wei, R.-A. Eichel, P. Notten, Interface aspects in all-solid-state Li-based batteries reviewed, *Adv. Energy Mater.* 11 (13) (2021), 2003939, <https://doi.org/10.1002/aenm.202003939>.
- J. Um, S.-H. Yu, Unraveling the mechanisms of lithium metal plating/stripping via in situ/operando analytical techniques, *Adv. Energy Mater.* 11 (27) (2021), 2003004, <https://doi.org/10.1002/aenm.202003004>.
- J. Lewis, J. Tippens, F. Cortes, M. McDowell, Chemo-mechanical challenges in solid-state batteries, *Trends Chem.* 1 (9) (2019) 845–857, <https://doi.org/10.1016/j.trechm.2019.06.013>.
- Z. Wang, J. Lee, H. Xin, L. Han, N. Grillon, D. Guy-Bouyssou, E. Bouyssou, M. Proust, Y. Meng, Effects of cathode electrolyte interfacial (CEI) layer on long term cycling of all-solid-state thin-film batteries, *J. Power Sources* 324 (2016) 342–348, <https://doi.org/10.1016/j.jpowsour.2016.05.098>.
- K. He, S. Cheng, J. Hu, Y. Zhang, H. Yang, Y. Liu, W. Liao, D. Chen, C. Liao, X. Cheng, Z. Lu, J. He, J. Tang, R. Li, C. Liu, In-situ intermolecular interaction in composite polymer electrolyte for ultralong life quasi-solid-state lithium metal batteries, *Angew. Chem. Int. Ed.* 60 (21) (2021) 12116–12123, <https://doi.org/10.1002/anie.202103403>.
- J. Bae, X. Zhang, X. Guo, G. Yu, A general strategy of anion-rich high-concentration polymeric interlayer for high-voltage, all-solid-state batteries, *Nano Lett.* 21 (2) (2021) 1184–1191, <https://doi.org/10.1021/acs.nanolett.0c04959>.
- J. Wang, X. Yan, Z. Zhang, R. Guo, H. Ying, G. Han, W.-Q. Han, Rational design of an electron/ion dual-conductive cathode framework for high-performance all-solid-state lithium batteries, *ACS Appl. Mater. Interfaces* 12 (37) (2020) 41323–41332, <https://doi.org/10.1021/acsami.0c10463>.
- L. Wang, R. Xie, B. Chen, X. Yu, J. Ma, C. Li, Z. Hu, X. Sun, C. Xu, S. Dong, T.-S. Chan, J. Luo, G. Cui, L. Chen, In-situ visualization of the space-charge-layer effect on interfacial lithium-ion transport in all-solid-state batteries, *Nat. Commun.* 11 (1) (2020) 5889, <https://doi.org/10.1038/s41467-020-19726-5>.
- C. Wang, L. Zhang, H. Xie, G. Pastel, J. Dai, Y. Gong, B. Liu, E. Wachsman, L. Hu, Mixed ionic-electronic conductor enabled effective cathode-electrolyte interface in all solid state batteries, *Nano Energy* 50 (2018) 393–400, <https://doi.org/10.1016/j.nanoen.2018.05.062>.
- S. Mu, W. Huang, W. Sun, N. Zhao, M. Jia, Z. Bi, X. Guo, Heterogeneous electrolyte membranes enabling double-side stable interfaces for solid lithium batteries, *J. Energy Chem.* 60 (2021) 162–168, <https://doi.org/10.1016/j.jechem.2020.12.026>.
- H. Li, Y. Du, X. Wu, J. Xie, F. Lian, Developing “polymer-in-salt” high voltage electrolyte based on composite lithium salts for solid-state Li metal batteries, *Adv. Funct. Mater.* 31 (41) (2021) 2103049, <https://doi.org/10.1002/adfm.202103049>.
- Z. Lv, Q. Zhou, S. Zhang, S. Dong, Q. Wang, L. Huang, K. Chen, G. Cui, Cyano-reinforced in-situ polymer electrolyte enabling long-life cycling for high-voltage lithium metal batteries, *Energy Storage Mater.* 37 (2021) 215–223, <https://doi.org/10.1016/j.ensm.2021.01.017>.
- M. Sun, Z. Zeng, L. Peng, Z. Han, C. Yu, S. Cheng, J. Xie, Ultrathin polymer electrolyte film prepared by in situ polymerization for lithium metal batteries, *Mater. Today Energy* 21 (2021), 100785, <https://doi.org/10.1016/j.mtener.2021.100785>.
- Y. Ruan, Y. Lu, Y. Li, C. Zheng, J. Su, J. Jin, T. Xiu, Z. Song, M. Badding, Z. Wen, A 3d cross-linking lithiophilic and electronically insulating interfacial engineering for garnet-type solid-state lithium batteries, *Adv. Funct. Mater.* 31 (5) (2021) 2007815, <https://doi.org/10.1002/adfm.202007815>.
- J. Zhang, J. Li, H. Zhai, G. Tan, X. Tang, One-step processing of soft electrolyte/metallic lithium interface for high-performance solid-state lithium batteries, *ACS Appl. Energy Mater.* 3 (7) (2020) 6139–6145, <https://doi.org/10.1021/acs.aem.0c01470>.
- Y. Jiang, Z. Wang, C. Xu, W. Li, Y. Li, S. Huang, Z. Chen, B. Zhao, X. Sun, D. Wilkinson, J. Zhang, Atomic layer deposition for improved lithiophilicity and solid electrolyte interface stability during lithium plating, *Energy Storage Mater.* 28 (2020) 17–26, <https://doi.org/10.1016/j.ensm.2020.01.019>.
- C. Wang, Y. Zhao, Q. Sun, X. Li, Y. Liu, J. Liang, X. Li, X. Lin, R. Li, K. Adair, L. Zhang, R. Yang, S. Lu, X. Sun, Stabilizing interface between $\text{Li}_{10}\text{SnP}_2\text{S}_{12}$ and Li metal by molecular layer deposition, *Nano Energy* 53 (2018) 168–174, <https://doi.org/10.1016/j.nanoen.2018.08.030>.
- A. Kato, A. Hayashi, M. Tatsumisago, Enhancing utilization of lithium metal electrodes in all-solid-state batteries by interface modification with gold thin films, *J. Power Sources* 309 (2016) 27–32, <https://doi.org/10.1016/j.jpowsour.2016.01.068>.
- S. Xu, D. McOwen, C. Wang, L. Zhang, W. Luo, C. Chen, Y. Li, Y. Gong, J. Dai, Y. Kuang, C. Yang, T. Hamann, E. Wachsman, L. Hu, Three-dimensional, solid-state mixed electron-ion conductive framework for lithium metal anode, *Nano Lett.* 18 (6) (2018) 3926–3933, <https://doi.org/10.1021/acs.nanolett.8b01295>.
- H.-J. Ha, E.-H. Kil, Y. Kwon, J. Kim, C. Lee, S.-Y. Lee, UV-curable semi-interpenetrating polymer network-integrated, highly bendable plastic crystal composite electrolytes for shape-conformable all-solid-state lithium ion batteries, *Energy Environ. Sci.* 5 (4) (2012) 6491–6499, <https://doi.org/10.1039/C2EE03025J>.
- Q. Li, X. Zhang, J. Peng, Z. Wang, Z. Rao, Y. Li, Z. Li, C. Fang, J. Han, Y. Huang, Engineering a high-voltage durable cathode/electrolyte interface for all-solid-state lithium metal batteries via in situ electropolymerization, *ACS Appl. Mater. Interfaces* 14 (18) (2022) 21018–21027, <https://doi.org/10.1021/acsami.2c02731>.
- H. An, Q. Liu, J. An, S. Liang, X. Wang, Z. Xu, Y. Tong, H. Huo, N. Sun, Y. Wang, Y. Shi, J. Wang, Coupling two-dimensional fillers with polymer chains in solid polymer electrolyte for room-temperature dendrite-free lithium-metal batteries, *Energy Storage Mater.* 43 (2021) 358–364, <https://doi.org/10.1016/j.ensm.2021.09.019>.
- Y. Zhang, C. Kim, W. Song, S.-J. Chang, H. Kim, J. Park, S. Hu, K. Zhao, S. Lee, Ultrahigh active material content and highly stable Ni-rich cathode leveraged by

oxidative chemical vapor deposition, *Energy Storage Mater.* 48 (2022) 1–11, <https://doi.org/10.1016/j.ensm.2022.03.001>.

- [26] G.-L. Xu, Q. Liu, K. Lau, Y. Liu, X. Liu, H. Gao, X. Zhou, M. Zhuang, Y. Ren, J. Li, M. Shao, M. Ouyang, F. Pan, Z. Chen, K. Amine, G. Chen, Building ultraconformal protective layers on both secondary and primary particles of layered lithium transition metal oxide cathodes, *Nat. Energy.* 4 (6) (2019) 484–494, <https://doi.org/10.1038/s41560-019-0387-1>.
- [27] H. Meng, D. Perepichka, M. Bendikov, F. Wudl, G. Pan, W. Yu, W. Dong, S. Brown, Solid-state synthesis of a conducting polythiophene via an unprecedented heterocyclic coupling reaction, *J. Am. Chem. Soc.* 125 (49) (2003) 15151–15162, <https://doi.org/10.1021/ja037115y>.
- [28] Y. Cheng, J. Shu, L. Xu, Y. Xia, L. Du, G. Zhang, L. Mai, Flexible nanowire cathode membrane with gradient interfaces and rapid electron/ion transport channels for solid-state lithium batteries, *Adv. Energy Mater.* 11 (12) (2021) 2100026, <https://doi.org/10.1002/aenm.202100026>.
- [29] H. Huo, Y. Chen, R. Li, N. Zhao, J. Luo, J. Silva, R. Mücke, P. Kaghazchi, X. Guo, X. Sun, Design of a mixed conductive garnet/Li interface for dendrite-free solid lithium metal batteries, *Energy Environ. Sci.* 13 (1) (2020) 127–134, <https://doi.org/10.1039/C9EE01903K>.
- [30] H. Duan, J. Zhang, X. Chen, X.-D. Zhang, J.-Y. Li, L.-B. Huang, X. Zhang, J.-L. Shi, Y.-X. Yin, Q. Zhang, Y.-G. Guo, L. Jiang, L.-J. Wan, Uniform nucleation of lithium in 3D current collectors via bromide intermediates for stable cycling lithium metal batteries, *J. Am. Chem. Soc.* 140 (51) (2018) 18051–18057, <https://doi.org/10.1021/jacs.8b10488>.



Hongxu Zhou is currently a postgraduate student at University of Science and Technology Liaoning, China. She obtained her B.S. degree from the University of Science and Technology Liaoning in 2021. Her current research focus on solid-state Li-S batteries.



Hongyang Li is currently a Ph.D. candidate at University of Science and Technology Liaoning, China. He obtained his B.S. degree from Eastern Liaoning University in 2018. His current research focus on the regulation of ion transport at anode-electrolyte interface for all-solid-state batteries.



Jingang Zheng is currently a Ph.D student at University of Science and Technology Liaoning, China. His current research focus on energy storage materials, solid-state lithium metal battery electrolyte-interface design and all-solid-state battery design.



Lixiang Li is a professor of University of Science and Technology Liaoning, China. She received her Ph.D in material science at Institute of Metal Research, Chinese Academy of Sciences in 2005 supervised by Prof. Hui-Ming Cheng. She had ever worked as a postdoctoral fellow at Tohoku University and a visiting scholar at the University of Michigan (Ann Arbor). Her current research interests include synthesis and electrochemical characteristics in advanced carbon materials/carbon-based composites.



Shaojun Liu is currently a Ph.D student at University of Science and Technology Liaoning, China. His research focus on the development and industrialization of lithium battery cathode materials, particularly phosphate cathode materials LFP and LMFP.



Guangshen Jiang is an associate professor of University of Science and Technology Liaoning, China. He received his Ph.D in materials science from Northwestern Polytechnical University in 2021. His current research involves the design and synthesis of solid-state electrolyte for metal batteries and the artificial interphase for dendrite modulation and suppression.



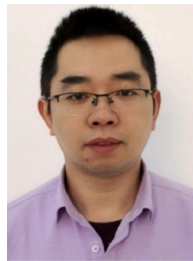
Hao Huang is currently a Ph.D student at University of Science and Technology Liaoning, China. His research focuses on the rational design of high-voltage electrolytes for lithium-ion batteries.



Han Zhang received his Ph.D. degree from Dalian University of Technology in 2019. Then he joined University of Science and Technology Liaoning, China, as an associate professor of Applied Chemistry since 2019. His research focuses on the fabrication and characterization of carbon nanomaterials with the applications in catalysis and energy storage. He has published over 10 papers in related fields.



Xin Geng is currently an associate professor in University of Science and Technology Liaoning, China. He obtained his Ph.D. in Department of Applied Chemistry with Professor Zhiyuan Tang at Tian Jin University in 2004, followed by a period of postdoctoral research in the Institute of Metal Research, Chinese Academy of Sciences. He joined University of Science and Technology Liaoning as an Associate Professor in 2007. His current research interests focus on the design, preparation, and applications of Lithium-ion ternary electrode materials.



Chengguo Sun received his Ph.D degree in chemical engineering and technology at Nanjing University of Science and Technology, China in 2014. He was working as a postdoctoral researcher, cooperated with Prof. Feng Li as supervisor, at institute of Metal Research, Chinese Academy of Science. He currently working as a full professor at Nanjing University of Science and Technology and a part-time professor at University of Science and Technology Liaoning. His research interests are high-energy-density materials, electrocatalysts and all solid-state lithium-ion batteries, aiming at preparation of the energetic cyclo-pentazolates salts and the high ionic conductivity of solid-state electrolytes.



Baigang An is a professor of University of Science and Technology Liaoning, China. He received his Ph.D in Applied Chemistry at Tianjin University in 2003 supervised by Prof. Shi-zhe SONG. He had ever worked as a research fellow at Tohoku University and a visiting scholar at the University of Michigan (Ann Arbor). His current research interests include synthesis and application of nanomaterials in electrochemical storage and conversion of energy.